Passive margins getting squeezed in the mantle convection vice

Philippe Yamato, Laurent Husson, Thorsten W. Becker, Kevin Pedoja

Passive margins getting squeezed in the mantle convection vice

Philippe Yamato,[1] Laurent Husson,[1,2] Thorsten W. Becker,[3] and Kevin Pedoja[4]

Received 21 May 2013; revised 10 September 2013; accepted 16 October 2013.

[1] Passive margins often exhibit uplift, exhumation, and tectonic inversion. We speculate that the compression in the lithosphere gradually increased during the Cenozoic, as seen in the number of mountain belts found at active margins during that period. Less clear is how that compression increase affects passive margins. In order to address this issue, we design a 2-D viscous numerical model wherein a lithospheric plate rests above a weaker mantle. It is driven by a *mantle conveyor belt*, alternatively excited by a lateral downwelling on one side, an upwelling on the other side, or both simultaneously. The lateral edges of the plate are either free or fixed, representing the cases of free convergence, and collision (or slab anchoring), respectively. This distinction changes the upper mechanical boundary condition for mantle circulation and thus, the stress field. Between these two regimes, the flow pattern transiently evolves from a free-slip convection mode toward a no-slip boundary condition above the upper mantle. In the second case, the lithosphere is highly stressed horizontally and deforms. For a constant total driving force, compression increases drastically at passive margins if upwellings are active. Conversely, if downwellings alone are activated, compression occurs at short distances from the trench and extension prevails elsewhere. These results are supported by Earth-like models that reveal the same pattern, where active upwellings are required to excite passive margins compression. Our results substantiate the idea that compression at passive margins is in response to the underlying mantle flow that is increasingly resisted by the Cenozoic collisions.

Citation: Yamato, P., L. Husson, T. W. Becker, and K. Pedoja (2013), Passive margins getting squeezed in the mantle convection vice, *Tectonics*, *32*, doi:10.1002/2013TC003375.

1. Introduction

[2] Paleogeographic reconstructions [e.g., *Blakey*, 2008] suggest that the Earth had much less topographic relief during the time of maximum continental dispersion, during the Late Cretaceous. Since then, continents continuously contract, and the many Cenozoic mountain belts at active margins best record this worldwide change. However, not only the active margins are exposed to deformation, and mounting evidence suggests that passive margins also undergo contraction—yet more subtle—and they are now often colloquially referred to as *not-so-passive margins*.

[3] A range of arguments is indicative of gentle shortening at passive margins. First, elevation is often anomalously high with respect to the surrounding continent (>2000 m at short distances from the coastline) [e.g., *Japsen et al*., 2012a and Figure 1]. Second, passive margins are also rapidly uplifting, as indicated by abundant, widespread, Upper Cenozoic sequences of paleocoasts (e.g., marine terrace, beach-ridges, and coral terraces) developed on the coasts located in such settings [*Pedoja et al*., 2011 and Figure 1]) and post-rift marine sediments (for instance, in NE Brazil [*Morais Neto et al*., 2006; *Martill*, 2007] and West Greenland [*Piasecki et al*., 1992; *Japsen et al*., 2006]). Third, ubiquitous exhumation at passive margins occurs during the Cenozoic (Figure 1). A variety of examples are found, among others, in India [*Gunnell and Fleitout*, 1998]; in the South Atlantic in general [*Gallagher and Brown*, 1999], Western Africa [*Lavier et al*., 2001], Morocco [*Ghorbal et al*., 2008], Southern Africa [*Partridge and Maud*, 1987; *Brown et al*., 2002; *Roberts and White*, 2010] and Brazil [*Cobbold et al*., 2001; *Cogné et al*., 2011, 2012; *Japsen et al*., 2012b], in particular; in the North Atlantic in general [*Japsen and Chalmers*, 2000; *Cloetingh and Van Wees*, 2005; *Cloetingh et al*., 2008], Greenland [e.g., *Japsen et al*., 2006; *Thomson et al*., 1999; *Japsen et al*., 2012a], Barents Sea and the Alaskan north slope [*Green and Duddy*, 2010], Norway [*Lundin and Doré*, 2002; *Ritchie et al*., 2008], the British Isles [*Hillis et al*., 2008a; *Holford et al*., 2008, 2009; *Smallwood*, 2008], and North Sea basin [*Japsen*, 1998], in particular. As pointed out by *Japsen et al*. [2012a], exhumation generally follows a period of subsidence and only occurs long after breakup, and might even be episodic. Lastly, tectonic inversion affects many margins (Figure 1). Again, examples are found in Brazil [*Gomes Sant'Anna et al*., 1997; *Riccomini*

[1]Geosciences Rennes, UMR 6118 CNRS, Université de Rennes 1, Rennes, France.
[2]LPGN, UMR 6112 CNRSS, Université de Nantes, Nantes, France.
[3]Department of Earth Sciences, University of Southern California, Los Angeles, California, USA.
[4]M2C, UMR 6143 CNRS, Université de Caen, Caen, France.

Corresponding author: P. Yamato, Geosciences Rennes, UMR 6118 CNRS, Université de Rennes 1, Rennes, France. (philippe.yamato@univ-rennes1.fr)

0278-7407/13/10.1002/2013TC003375

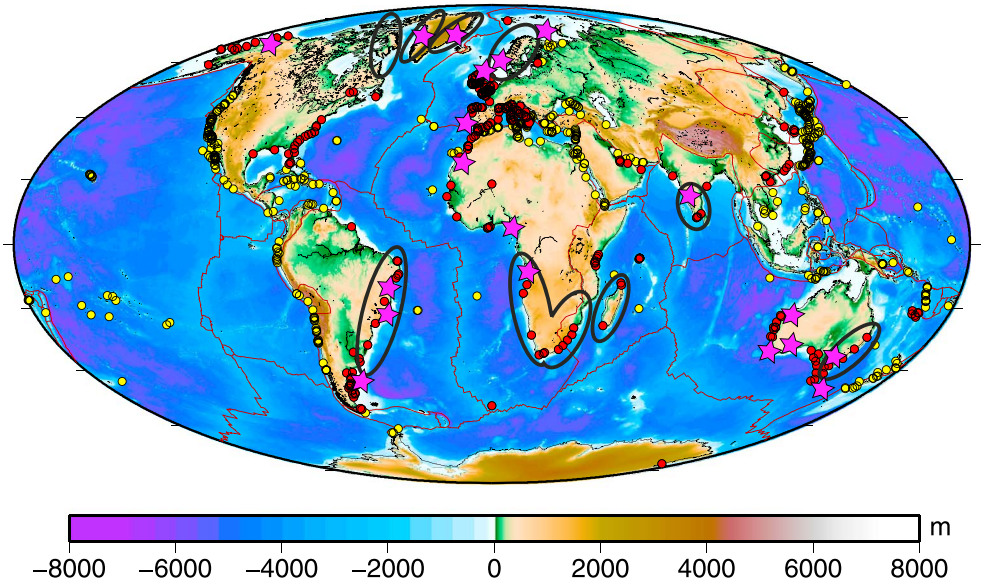

Figure 1. Synthetic map showing the following: (i) anomalously elevated passive margins (topography and black ellipses, after *Japsen et al*., 2012a), (ii) coastal sequence including the last interglacial maximum benchmark (125 ka) (dots, after *Pedoja et al*. [2011]; passive margins are plotted in red, others in yellow), and, (iii), exhumed and tectonically inverted passive margins during the Cenozoic (magenta stars, see text for details and references).

and Assumpcao, 1999; *Cobbold et al*., 2007; *Cogné et al*., 2011, 2012] and Patagonia [*Rodriguez and Littke*, 2001], in the British Isles [*Andersen and Boldreel*, 1995; *Lundin and Doré*, 2002; *Smallwood*, 2008] and in the North Atlantic [*Doré et al*., 1997], Norway [*Brekke*, 2000], West Africa [*Hudec and Jackson*, 2002; *Jackson et al*., 2005; *Briggs et al*., 2009], Moroccan Meseta [*Ghorbal et al*., 2008], India [*Gunnell and Fleitout*, 1998], Iberia [*Masson et al*., 1994; *Peron-Pinvidic et al*., 2008], and Australia [*Hillis et al*., 2008b; *Bishop and Goldrick*, 2000]. Here we refer to tectonic inversion when former normal faults are tectonically inverted and unambiguously reveal compression. Exhumation itself may not be as symptomatic and may be caused by mantle rather than lithospheric activity.

[4] Several mechanisms, for instance, dynamic support from the underlying mantle flow in West Africa [e.g., *Lithgow-Bertelloni and Silver*, 1998], flexure due to sedimentary loading [e.g., *Gunnell and Fleitout*, 1998], and enhanced erosion due to climate change [*Clift*, 2010] partially explain these observations on regional scales. In fact, such mechanisms satisfactorily explain uplift and exhumation but fail to explain tectonic inversions. Only subduction initiation at passive margins may trigger modest compression, uplift, and exhumation [e.g., *Nikolaeva et al*., 2010]. Moreover, because most margins appear affected in a similar fashion, these observations suggest a general process that applies at least at the scale of the Atlantic, where most passive margins are found at present, but likely also on global scales.

[5] Exhumation and tectonic inversion in many instances occur at conjugate margins (e.g., Brazil and Western Africa, [*Japsen et al*., 2012b] and the margins of the North Atlantic [*Japsen et al*., 2012a]). Even more intriguing is the fact that phases of tectonic inversion at passive margins appear to be coeval to periods of tectonic activity at their active counterparts. This is observed in South America [*Cobbold et al*., 2007] where the Peruvian, Incaic, Quechua phases of Andean deformation match the deformation at the Brazilian margin [*Cogné et al*., 2012], or Iberia where tectonic inversion is synchronous to the Alpine deformation [*Peron-Pinvidic et al*., 2008]. This observation suggests that a general process leads to compression at both margins. Plate tectonics and continental deformation are, of course, ultimately linked to mantle convection. Sublithospheric mantle tractions are thought to be relevant for relative plate motions, trench motions, and lithospheric deformation [e.g., *Steinberger et al*., 2001; *Becker and O'Connell*, 2001; *Conrad and Lithgow-Bertelloni*, 2002; *Lithgow-Bertelloni and Guynn*, 2004; *Husson*, 2012]. In the Indian Ocean [*Becker and Faccenna*, 2011], the South Atlantic [*Husson et al*., 2012], or along the entire global plate circuit [*Faccenna et al*., 2013], approximately cylindrical, whole mantle convection cells underneath the drifting plates successfully explain the time evolution of active orogens at convergent boundaries. These previous studies explored how mantle "conveyor belts" need to be simultaneously excited by active upwellings and downwellings, as opposed to large-scale return flow, in order to match the observed kinematics. Downwellings associated with subduction pull the plates trenchward and are therefore essentially a source of extension in the lithosphere. Conversely, if upwellings are located close to spreading centers ("ridges"), they can serve to push plates from ridges to trenches and are a source of compression. Of course, because of conservation of mass, an upwelling is necessarily associated to, at least, one downwelling (and vice versa) but the importance of their contributions is a matter of (i) focusing (slab-like, focused downwellings can be counterbalanced by upwellings that are either diffuse or localized, underneath oceanic ridges in particular); and (ii) their respective buoyancies that render them either active or passive. In the present-day plate configuration, upwellings, chiefly fuelled by the African superswell, appear

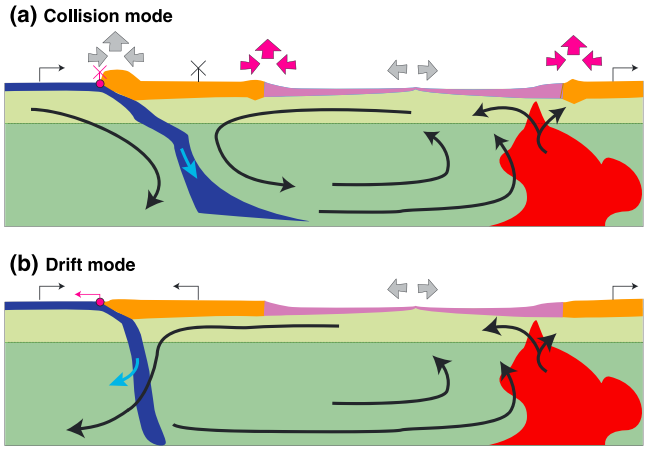

Figure 2. Sketch of the mantle convective cell flow in (a) collision mode and (b) drift mode. In the collision mode, the anchored slab does not retreat and prevents the trench-ward motion of the upper plate and is thus blocked. In drift mode, the subducting slab is retreating and accommodates the oceanic lithosphere convergence that can freely move. Thick black and blue arrows show mantle flow and slab motion, respectively. Thin black and magenta arrows correspond to the lithosphere and trench displacements, respectively. These thin arrows are replaced by crosses when the motion is zero with respect to the upwelling. Large grey and magenta arrows correspond to compressional and extensional areas at active and passive plate margins, respectively.

to significantly contribute to the force balance, and in particular compress the upper plates. The prominent consequence is the formation of compressive belts at active plate boundaries. Because upwellings and downwellings on each side of the convection cell combine together, it is the entire plate that rides the convection cell that likely undergoes compression (Figure 2a) and collateral damage may occur anywhere in the plate, including at passive margins. The relative contributions of the upwelling and downwelling force appear critical to the wholesale compression of the plate.

[6] Slab anchoring in the lower mantle modifies the flow pattern underneath the lithosphere. If rollback freely occurs, or if it occurs faster than the oceanward motion of the upper plate, mantle flow does not dramatically interfere with the slab. Conversely, if the mantle flows faster than rollback, the convection cell gets circumscribed by the downgoing slab, on the one hand, and by the upwelling, on the other hand (Figure 2b). This modifies the state of stress in the lithosphere, and the latter will promote compression in the upper plate, at least at its active margin [*Jolivet and Faccenna*, 2000]. However, we speculate that the same regime applies to the passive counterpart. We thereafter refer to these two end members as drift mode and collision mode, respectively.

[7] Post-rift tectonic inversion at passive margins has been addressed kinematically [e.g., *Leroy et al.*, 2004], where deformation reacts to an imposed convergence rate. Here we emphasize the role of basal drag excited by mantle flow, alternatively driven by upwellings and downwellings. We therefore set out to test how upwelling and downwelling forces act on the lithosphere depending on the configuration of the lithospheric plates and to explore the required conditions that promote contraction at passive margins, when the system switches from drift to collision mode.

[8] We only consider large-scale active upwellings and downwellings. Ridge-push, and its temporal variations, are assumed to be insufficient to trigger phases of compression. We thus only test the hypothesis that compression is triggered by large-scale mantle flow and ignore lithosphere-scale processes. This study possibly best applies to the South Atlantic system, an idealized version of which we used to design the experimental setup. However, the obtained results are also applicable to other cases (e.g., Australia and Africa, see Figure 1) where the main lines of dynamics appear to be akin to that of the South Atlantic in many aspects.

2. Numerical Model

2.1. Equations Solved

[9] In our numerical code (see full description in *Yamato et al.* [2012]), we solve the Stokes equations in 2-D (equations (1) and (2)) subject to the incompressibility constraint (equation (3))

$$-\frac{\partial P}{\partial x}+\frac{\partial \tau_{xx}}{\partial x}+\frac{\partial \tau_{xz}}{\partial z}=0, \tag{1}$$

$$-\frac{\partial P}{\partial z}+\frac{\partial \tau_{zz}}{\partial z}+\frac{\partial \tau_{zx}}{\partial x}=\rho g, \tag{2}$$

$$\frac{\partial Vx}{\partial x}+\frac{\partial Vz}{\partial z}=0, \tag{3}$$

where P, τ_{ij}, ρ, and g correspond to the pressure, deviatoric stress tensor, density, and gravitational acceleration, respectively. V_x and V_z are the two components of the velocity vector in a 2-D (x, z) Cartesian coordinate system. These equations are solved numerically on a Eulerian-staggered grid by a finite difference method [*Gerya and Yuen*, 2003, 2007]. Field properties such as viscosities and densities are originally set on Lagrangian particles that can be advected following a Runge-Kutta scheme within the model domain. The numerical scheme was already intensively tested [*Yamato et al.*, 2012] and is well suited for problems involving linear viscous materials as will be used here throughout. Since we are interested in the first-order dynamics of passive margin deformation, we do not invoke more complex rheologies or

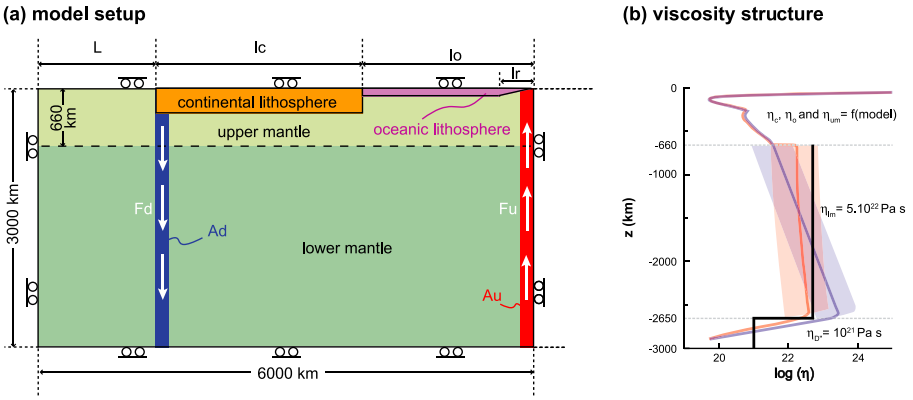

Figure 3. Initial configuration of the model. (a) Model setup. L: length of mantle space between the left-hand side of the box and the continental lithosphere; l_c: length of continental lithosphere; l_o: length of oceanic lithosphere; l_r: length corresponding to the thinning of the lithosphere due to the ridge; F_d: downwelling force; F_u: upwelling force. These buoyancy forces are implemented by setting variable densities in the red and blue columns. The area of the columns is A_d and A_u for the downwelling and the upwelling force, respectively. See also text for details. (b) Viscosity structure. η_c, η_o, and η_{um} correspond to the viscosity of the continental lithosphere, oceanic lithosphere, and upper mantle, respectively. The viscosity of the lower mantle corresponds to a simplified profile (black line). The viscosity models from *Cizkova et al.* [2012] are also provided (Family-A model in red and Family-B model in blue) as references.

geometries which introduce necessarily new parameters (e.g., temperature and stress dependent rheologies, subduction angle, passive margin morphology, oceanic lithosphere age, etc.) that would likely only blur our analysis. This also ensures the reproducibility of our results that can be easily tested by any code-solving Stokes equations with free-slip boundary conditions.

2.2. Model Setup

[10] Our model approximates a part of the Earth's mantle located between the core-mantle boundary and the surface. Our model geometry is purposely kept as simple as possible (Figure 3a). The Cartesian box is 6000 km wide and 3000 km deep. The grid resolution used is of 601 × 301 nodes which corresponds to a spatial resolution of 10 km. We consider this resolution sufficient because (i) the wavelength of the expected perturbations are typically one order of magnitude higher and (ii) we performed resolution tests; by increasing the resolution by factors of 2 and 4 that lead to very similar velocity fields. All the mechanical boundary conditions are free slip and all the viscosities in our model are linear viscous.

[11] A continental lithosphere adjacent to an oceanic lithosphere at its right-hand side is located on the top of the model (Figure 3a). The left-hand side of the continental lithosphere rests above a body of negative buoyancy that models a downwelling zone (slab in subduction zone). It integrates to a downward force F_d. Tuning the density contrast between the whole mantle and this prescribed domain (in blue in Figure 3a) sets the value of F_d. At the opposite, the right side of the oceanic lithosphere rests above a domain of positive buoyancy, which integrates to an upward force F_u and that similarly models an upwelling zone (in red in Figure 3a). In this last case, the density difference between the upwelling material and the mantle is then negative. These two forces (F_d and F_u) are the only driving forces in our model, and they are balanced by viscous dissipation in the mantle. We do not consider other effects, whose contributions (e.g., details of slab bending, interplate friction as resisting forces, and gravitational sliding of the cooling oceanic lithosphere ("ridge push") as driving forces) may explain local departures from the general behavior that we test here because our model is more conceptual than applied to a given setting.

[12] The net values of these internal forces are, however, not well known. For the South Atlantic, the sum of F_d and F_u is supposed to be on the order of $\sim 10^{13}\,\mathrm{N\,m^{-1}}$ [*Husson et al.*, 2012], for example. To facilitate comparison between all of our models, we decided to keep the net force ($F_u + F_d$) that excites the mantle convection cell constant. In that way, this total force can be easily distributed between the upwelling and/or downwellings (see section 3.2). This total force is somewhat arbitrarily set to $2 \cdot 10^{13}\,\mathrm{N\,m^{-1}}$ in all our models, corresponding to typical plate tectonic value (slab pull, [see e.g., *Turcotte and Schubert*, 1982]). This choice does not restrict generality: since everything is linear in our experiments, should this force be modified by a given factor, our quantitative results would scale accordingly, but our conclusions would not be altered. In addition, the same results can be obtained for other values by adjusting the viscosities by an appropriate factor. In that sense, we could have opted for a dimensionless analysis, but for an easiest comparison with natural data, we decided to keep dimensional values.

[13] In our models, continental and oceanic lithospheres are modeled by rectangular bodies. The "ridge side" of the oceanic lithosphere ends as a triangle over 500 km (i.e., l_r = 500 km, Figure 3a). The oceanic lithosphere is not attached to the right-hand side of the box, for one upper mantle cell separates it from the model box edge. This ensures that the lithosphere is free to move laterally and is not affected by the free-slip boundary condition imposed at the right side, which would impose $V_x = 0$ at the lithosphere edge. Setting different values for l_r only modifies the results by no more than $1\,\mathrm{mm\,yr^{-1}}$ and yields overall very similar kinematics. For this reason, we thus chose to stick to a value of l_r set to 500 km in all our computations.

[14] The influence of the thickness of both the oceanic and continental lithospheres is not presented here either for two reasons. First, by testing different values for the thickness of the oceanic lithosphere and considering that the continental lithosphere thickness is larger than the oceanic one, the results are identical. Second, since these parameters can be inferred from geophysical data, they do not constitute a real unknown parameter. We thus fixed typical thicknesses to 200 km and 100 km [e.g., *Conrad and Lithgow-Bertelloni*, 2006] for the continental and the oceanic lithosphere, respectively. The width of the continental lithosphere is similarly set in all our models to 2000 km.

[15] In our model, the density is generally uniform and set to $\rho_{\mathrm{ref}} = 3250\ \mathrm{kg\,m^{-3}}$ everywhere in the model box. Density differences are only assigned to the upwelling and the downwelling zones that drive, by buoyancy, the convection cell (Figure 3a). The density value in the upwelling (ρ_u) and in the downwelling (ρ_d) areas depends on the buoyancy force applied and are expressed as follows:

$$\rho_u = \rho_{\mathrm{ref}} - \frac{F_u}{\rho_{\mathrm{ref}} \cdot g \cdot A_u} \tag{4}$$

$$\rho_d = \rho_{\mathrm{ref}} + \frac{F_d}{\rho_{\mathrm{ref}} \cdot g \cdot A_d} \tag{5}$$

where F_u and F_d correspond to the absolute values of the upwelling and downwelling forces, respectively, and g is the gravitational acceleration (set to $9.81\ \mathrm{m\,s^{-2}}$). These upwelling and downwelling forces are thus evenly distributed over the surfaces A_u and A_d, respectively (see Figure 3a). Here we focus on the tractions caused by convective flow in the mantle. However, we are aware that the complete lithospheric stress field will also have contributions due to lateral variations in the gravitational potential energy due to differences in the vertical density structure above the compensation depth. In particular, the mean continental plate stress state is strongly affected by the density of the lithospheric mantle and crustal thickness [*Fleitout and Froidevaux*, 1983]. Any such effects will be superimposed on the patterns we discuss here.

[16] The viscosity profile used in our models is presented in Figure 3b. The viscosity in the lower mantle corresponds to a very simplified profile: From 660 km to 2650 km depth, the viscosity is set to $\eta_{\mathrm{um}} = 5 \cdot 10^{22}$ Pa s. Below, the viscosity is set to 10^{21} Pa s (D″ layer). Experiments have also been done by using a B-family profile (see details in *Cizkova et al*. [2012]). However, since the results yield identical conclusions, we thus choose to use the simplest 1-D viscosity profile for this study. Above the lower mantle, the viscosities are not well resolved and therefore need to be tested (section 3.1). To simplify, we considered the viscosity of the continental lithosphere, of the oceanic lithosphere, and of the upper mantle as linear and constant. Implementing nonlinear rheologies would at the largest scales mainly affect rates but not patterns of mantle flow, and likely by an amount that is not critical to our aims of conceptual exploration [see e.g., *Becker*, 2006]. Our simplified rheology also implicitly discards the effect of slab stiffness that will modulate the surrounding mantle flow [e.g., *Conrad and Lithgow-Bertelloni*, 2002; *Loiselet et al*., 2010]. In fact, because there is no proper slab-like structure—besides the density of the negatively buoyant unit—the models where the downwelling zone is remote from the box edge correspond to a subduction zone that offers no resistance to the upper plate, i.e., a subduction zone where the rate of rollback adjusts to the rate at which the upper plate migrates toward the subduction zone. Conversely, models where the downwelling zone is at the box edge corresponds to a situation where the slab offers an absolute resistance to upper plate drift. These situations shall thus be considered as the two end members Earth-like regimes of subduction.

[17] The aim of our study is (i) to quantify the influence of the force balance between downwelling and upwelling on the deformation of the lithosphere, and (ii) to highlight the consequences of the current continental aggregation that, to some extent, corresponds to the transition from a continent that is free to ride over the mantle (drift mode) to a continent that is blocked by the adjacent subducting or colliding plates (collision mode). However, since it is impossible to address this problem without some knowledge of the viscosities of the lithospheres and upper mantle, they thus need to be constrained first. We thus proceed to test the influence of the upper mantle and of the continental/oceanic lithosphere viscosities.

3. Results

[18] As the natural observation described in section 1 corresponds to the actual state of the lithosphere, we first focused our study on the collision mode ($L = 0$, see Figure 3a). This configuration corresponds to the actual state of the South American plate blocked at its eastern margin by the subduction of the Nazca plate, anchored underneath the Andes [*Husson et al*., 2012]. This reference model will be used later for a study through time (in drift mode) by using different values for L (see Figure 3a). This allows us to constrain (i) the suitable radial viscosity structure and (ii) the force balance needed to match the model results (velocity and strain rate) with observations. These parameters will form the basis upon which we further elaborate our analysis of the time evolution of this system.

3.1. Setting Up the Radial Viscosity Structure

[19] In the collision mode, $L = 0$ and the lithosphere cannot move freely above the convection cell (see Figure 1a). As noted in section 1, the net driving force involved in this example amounts to $2 \cdot 10^{13}\ \mathrm{N\,m^{-1}}$. This total force is evenly distributed ($F_u = F_d = 10^{13}\ \mathrm{N\,m^{-1}}$). The influence of this partitioning of the total force is discussed later in section 3.2. Figure 4 shows the results obtained with an identical viscosity for both oceanic and continental lithospheres and a range of viscosities for the upper mantle.

[20] In such configurations, for an acceptable range of values of the upper mantle viscosity η_{um} (from 10^{19} to 10^{21} Pa s), the viscosity of the continental lithosphere η_{c} should be close to 10^{22} Pa s in order to get strain rates in the lithosphere that compare to the observations, for the Andes in particular. Indeed, in these models (i) the strain rate reaches its maximal value close to the collision area (corresponding to the Andes) and (ii) the second invariant strain rate profile is between 10^{-15} and $10^{-16}\ \mathrm{s^{-1}}$ over ~500 km width decreasing from the west to the east, which is comparable to the value inferred from the World Strain Rate Map (WSRM) of *Kreemer et al*. [2003]. For higher viscosities ($\eta_{\mathrm{c}} = \eta_{\mathrm{o}} = 10^{23}$ Pa s), deformation in the collision area becomes

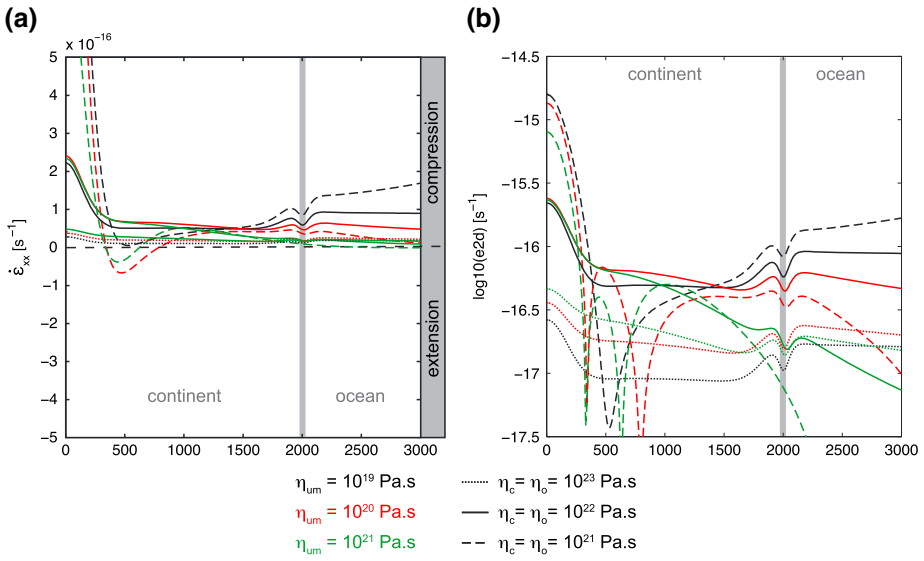

Figure 4. (a) Shortening rate $\dot{\varepsilon}_{xx}$ (horizontal component of the strain rate tensor) at the surface across the 3000 km long continental and oceanic lithospheres ($L = 0$ km, $l_c = 2000$ km, $F_d = F_u = 10^{13}$ N m^{-1}, see Figure 3a). Positive values of $\dot{\varepsilon}_{xx}$ correspond to compression. (b) Logarithm of the second invariant of the strain rate (e2d) along the same profile.

too small ($< 10^{-16}$ s^{-1}, Figure 4a) and the corresponding second invariant of the strain rate (Figure 4b, dotted lines) is low ($< 10^{-16}$ s^{-1}). Moreover, this leads to deformation at the passive margin with the same order of magnitude as that at the active margin, which is obviously not the case in reality. The second invariant of the strain rate at passive margins is close to zero in the WSRM because strain rates are much lower than that at the active margins. However, the World Strain Rate Map should, of course, be taken with caution because its usefulness is inherently limited to regions where there is sufficient (geodetic) data coverage, and this is generally not the case for passive margins.

[21] For lower continental lithosphere viscosities, deformation in the collisional area (Andes) is also high and extends over ~500 km width; however, these models yield unrealistic extension at the back (Figure 4a, dashed lines), which is also incompatible with the case of the South American plate in particular. This acceptable value of 10^{22} Pa s is in good agreement with values found for the effective viscosity of the deforming Andean lithosphere [e.g., *Husson and Ricard*, 2004]. As to the viscosity ratio between the lithosphere and upper mantle, our models show that it should be ~100 to produce both realistic strain rates of passive margins and a limited deformation of the oceanic lithosphere. For a higher viscosity ratio, no deformation of the passive margin occurs (Figure 4a, green lines). If, conversely, this viscosity ratio is too low, deformation of the oceanic lithosphere becomes higher than that at the passive margin, in disagreement with observations [e.g., *Kreemer et al.*, 2003]. Within the framework of our model simplifications, the average viscosity of the lithosphere is hence quite well constrained: the viscosity of the continental lithosphere has to be ~10^{22} Pa s and ~100 times that of the upper mantle. These values are in good agreement with those obtained from postglacial rebound and convection studies (see e.g., *Mitrovica and Forte*, 2004; and discussion in *Cizkova et al.* [2012]), even if lateral viscosity variations can trade-off with such average layer estimates [e.g., *Yoshida and Nakakuki*, 2009; *Ghosh et al.*, 2010].

[22] However, constant viscosity for both continental and oceanic lithosphere is problematic because in such a configuration, the strain rate in the oceanic lithosphere is higher than that at the passive margin (Figure 4a). Increasing the viscosity ratio between the oceanic and continental lithospheres yields more acceptable predictions. Results are

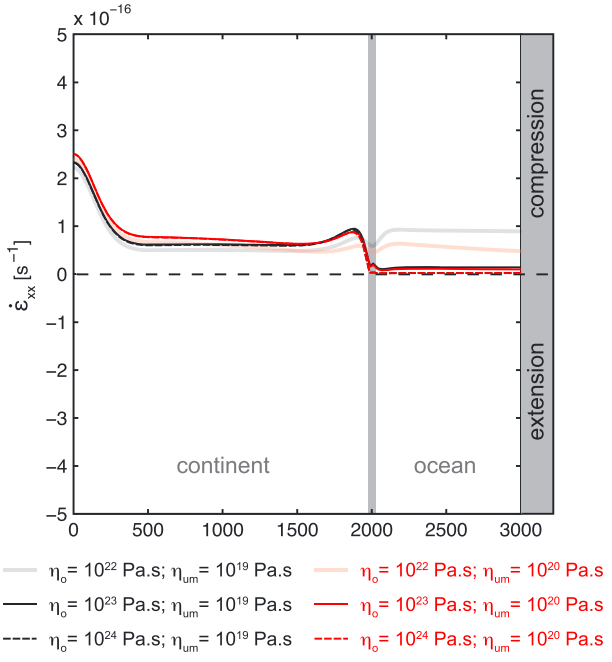

Figure 5. Horizontal component of the strain rate ($\dot{\varepsilon}_{xx}$) across the 3000 km long continental and oceanic lithospheres ($L = 0$ km and $l_c = 2000$ km, see Figure 3a), for a variety of oceanic η_o and upper mantle η_{um} viscosities. The viscosity of the continental lithosphere η_c is set to 10^{22} Pa s.

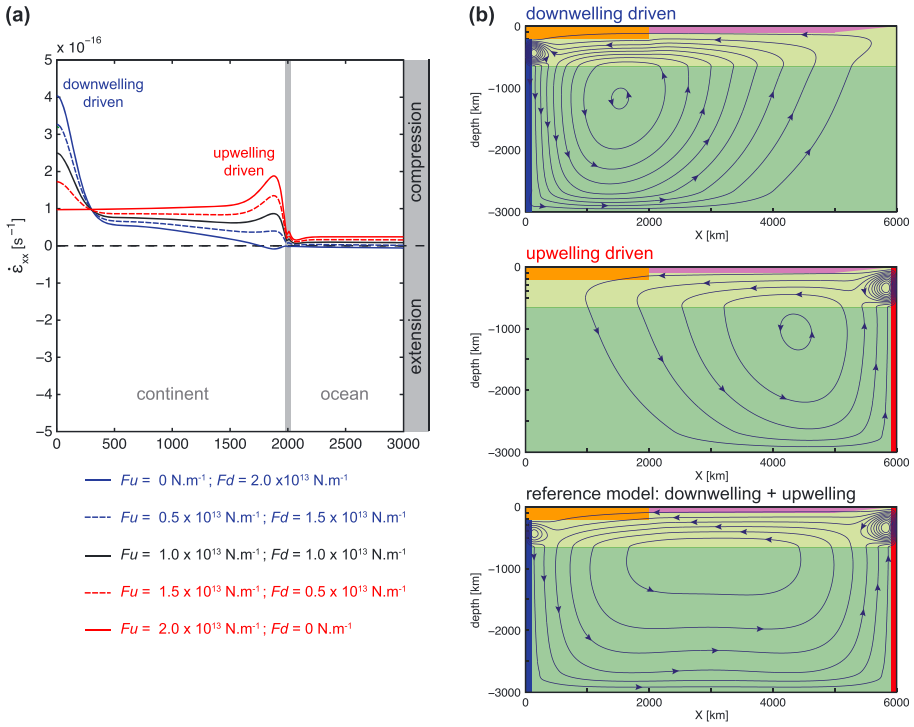

Figure 6. (a) Strain rate at the surface across the 3000 km long continental and oceanic lithospheres ($L = 0$ km and $l_c = 2000$ km, see Figure 3a). (b) Streamlines obtained for the downwelling driven model ($F_u = 0$ N m^{-1}, $F_d = 2 \cdot 10^{13}$ N m^{-1}), the upwelling driven model ($F_u = 2 \cdot 10^{13}$ N m^{-1}, $F_d = 0$ N m^{-1}), and the reference model ($F_u = 10^{13}$ N m^{-1}, $F_d = 10^{13}$ N m^{-1}).

shown in Figure 5 for different viscosity values for the oceanic lithosphere (from 10^{22} to 10^{24} Pa s) and upper mantle (10^{19} and 10^{20} Pa s).

[23] These results show that regardless of the absolute viscosity of the oceanic lithosphere, similar results are obtained provided that the oceanic lithosphere is more viscous than the continental counterpart. This choice is plausible given the globally uneven distribution of intraplate seismicity [e.g., *Gordon*, 2000] and the rheological inference that the strength of the oceanic lithosphere at a passive margin should be higher than the continental one for ages older than ~100 Myr [e.g., *Kohlstedt et al.*, 1995]. Indeed, similar viscosities have been used by *Leroy et al.* [2004] to explore the deformation at passive margins.

[24] In summary, these results show that—at least in a collisional mode—the best parameters that yield results that are in agreement with the observations are: (i) a viscosity for the continental lithosphere (η_c) of about 10^{22} Pa s, (ii) a stiffer oceanic than continental lithosphere ($\eta_o > \eta_c$), and (iii) an upper mantle viscosity (η_{um}) in the range from 10^{19} to 10^{20} Pa s. We accordingly use $\eta_c = 10^{22}$ Pa s; $\eta_o = 10^{23}$ Pa s and $\eta_{um} = 10^{20}$ Pa s for our reference model.

3.2. Influence of the Force Balance: Upwellings Versus Downwellings

[25] We build upon our reference experiment to explore the respective influence of the downwelling and upwelling forces. In a collisional mode, our reference model is driven by a mantle convection cell excited by both the lateral downwelling and the upwelling ($F_u = F_d = 10^{13}$ N m^{-1}). To test the respective effect of the downwelling and the upwelling forces on the strain rate profile in the lithosphere, we modified their respective contribution but kept the net sum of these forces unchanged throughout all models.

[26] The strain rate profiles in the lithosphere are presented in Figure 6a and the streamlines of global mantle flow in Figure 6b. Increasing the downwelling force relative to the upwelling force leads to an increase of the compressive deformation on the active margin side and to a decrease of the compressive deformation on the passive margin side. More interestingly, if the upwelling force is completely switched off, the passive margin undergoes extension. Conversely, increasing the upwelling force compared to the downwelling force fosters compression at the passive margin. Strain rates are equal at both passive and active margins when the upwelling force amounts to ~1/3 of the downwelling force.

[27] From these results, we suggest that upwellings play a major role on the stress regime of the lithosphere located above the convection cell. In the absence of upwellings at the ridge end of the cell, passive margins are in extension because upwellings push plates and thus only add compression. Downwellings conversely pull the plates toward the subduction zones. In principle, by doing so, they add extension. But these observations only hold at large distances from the trench; in the mantle wedge next to the trench, corner flow (Figure 6b) causes sublithospheric horizontal shear stress to increase away from the trench, up to a certain distance that scales with the thickness of the upper mantle. This flow compresses the lithosphere next to the trench; a mechanism that has been previously envisioned as a driver for the Andean orogeny [e.g., *Wdowinski and O'Connell*, 1991]. Moreover, the ratio between upwelling and downwelling

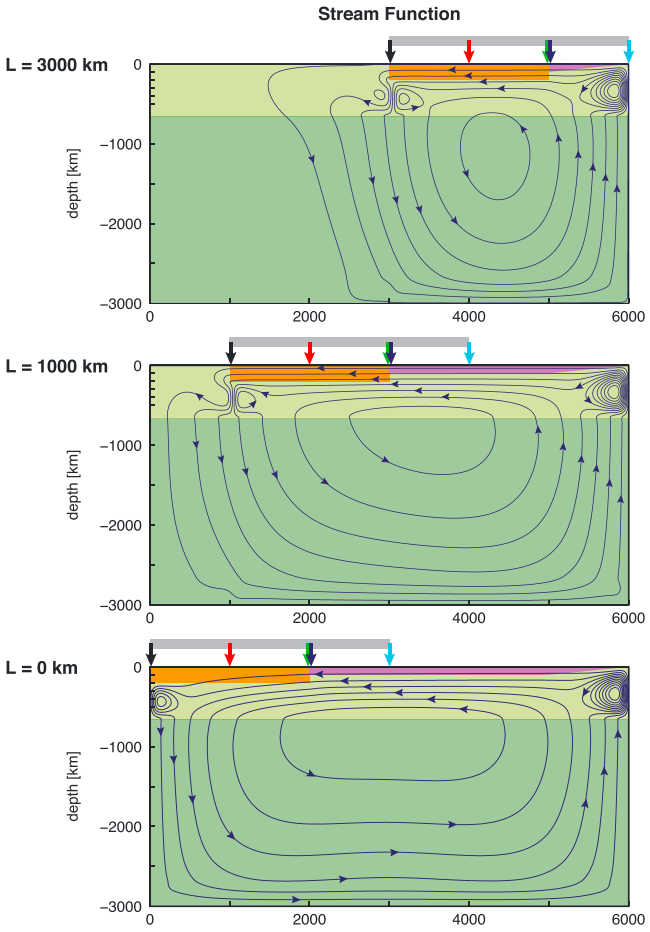

Figure 7. Streamlines (in blue) for three models where the only difference is the distance (L) from the left-hand side of the box to the continental lithosphere. Arrows with different colors correspond to the locations of the different vertical profiles shown in Figure 8. The gray segment shows the location of the strain profiles of Figure 9.

forces should be close to 1 and larger than ~1/3 to produce both high strain rates in the collision zone (typically the Andes) and smaller rates at passive margins, in agreement with general observations, and with the South American plate in particular.

[28] To fit with observations of the strain rate occurring both at the active and at the passive margin, the preferred setting in the collision mode seems to be the one where upwellings and downwellings act in comparable fractions of the net driving force. In order to test the evolution of the strain regime through time between the drift mode and the collision mode, we thus choose to use equal upwelling and downwelling forces (i.e., $F_u = F_d = 10^{13}\,\mathrm{N\,m^{-1}}$).

3.3. Drift Versus Collision Mode

[29] At the opposite of the collision mode, where the continental lithosphere is blocked by an anchored subducting plate (or similarly, by a collision), the drift mode corresponds to a case of free motion of the lithosphere located over the convection cell (see Figure 2). To address the consequences of the transition from drift to collision mode, we performed experiments by placing the continental lithosphere and the downwelling at different distances (L) from the left-hand side of our model box (see Figure 3a). These instantaneous experiments mimic the time evolution of the dynamics of the system during this transition.

[30] Figure 7 shows the streamlines obtained for $L = 3000$ km, $L = 1000$ km (i.e., in drift mode), and $L = 0$ km (i.e., in collision mode). Viscosity parameters are the same as for the reference model ($\eta_{um} = 10^{20}$ Pa s, $\eta_c = 10^{22}$ Pa s, and $\eta_o = 10^{23}$ Pa s) and the force balance is set as follows: $F_u = 10^{13}\,\mathrm{N\,m^{-1}}$ and $F_d = 10^{13}\,\mathrm{N\,m^{-1}}$. The size of the convection cell increases with time when L is decreasing. Consequently, since the total force in the system is kept constant ($F_u + F_d = 2 \cdot 10^{13}\,\mathrm{N\,m^{-1}}$), the volume of mantle that enters in motion increases with the dimension of the cell, and the velocity in the horizontal direction of the lithosphere located over the mantle is then decreasing. This can be observed on Figure 8 where vertical profiles of the horizontal velocity are provided for the three different cases, at different locations in the model (see arrows on Figure 7). Indeed, at the surface, the velocity (V_x) decreases from $L = 3000$ km to $L = 1000$ km (difference between dashed and dotted lines on Figure 8).

[31] Figures 7 and 8 show that the flow below the lithosphere is dramatically different between these two modes. In drift mode (dashed and dotted lines, Figure 8), mantle circulation resembles a Poiseuille flow with a free surface. As the lithosphere approaches the end wall and therefore is no longer free to move laterally, the upper mantle circulation gradually converts into a Poiseuille flow in the strict sense,

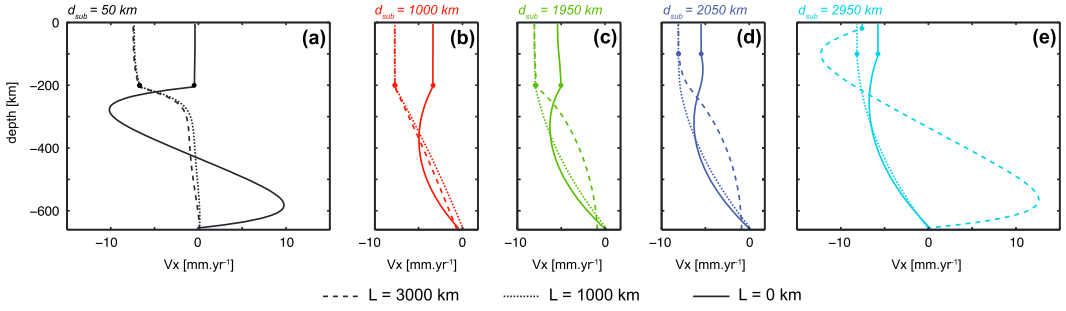

Figure 8. Vertical profiles through the model box showing the evolution of the horizontal velocity with time when the distance L is decreasing. These profiles are computed at different distances (d_{sub}) from the left edge of the continental lithosphere (subduction zone). Colors correspond to these locations represented by color arrows in Figure 7. (a), (b), and (c) Profiles that pass across the continental lithosphere and (d) and (e) profiles that pass across the oceanic lithosphere. The dots correspond to the lithosphere-upper mantle transition.

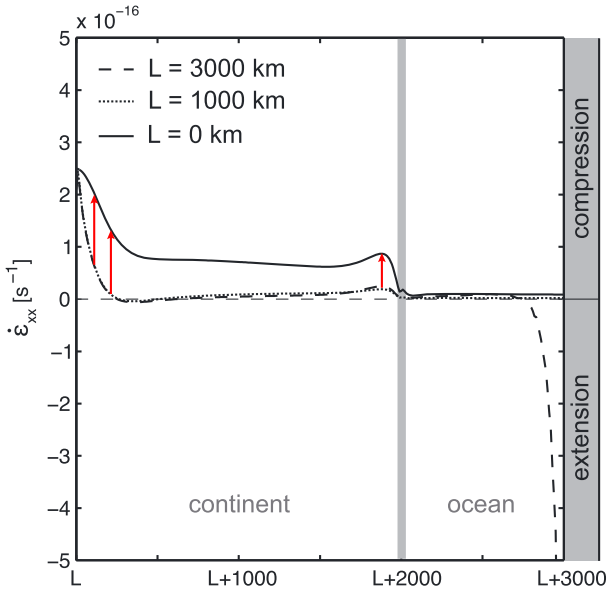

Figure 9. Horizontal component of the strain rate ($\dot{\varepsilon}_{xx}$) at the surface across the 3000 km long continental and oceanic lithospheres. Red arrows show the jump that occurs at the transition from drift mode to collision mode.

between two units that deform at much slower rates, namely the lithosphere and the lower mantle. This behavior is akin to the transition from a mobile lid to a sluggish lid regime of mantle convection. The horizontal velocities at the surface are also different along the lithosphere, indicating that large deformation occurs. The mantle flow just below the lithosphere switches from a convex shape oriented toward the upwelling (convex-right in Figure 8, dashed and dotted lines) to a convex shape oriented toward the downwelling (convex-left in Figure 8, solid line) when the system switches from drift to collision mode.

[32] Since it reflects the variation of the horizontal velocity field in the lithosphere, the same conclusions are achieved when plotting the resulting horizontal strain rate profile in the lithosphere (Figure 9). This graph clearly shows that strain rates are boosted at the transition between the drift mode and the collision mode (red arrows). In drift mode, large deformation occurs at the active margin, but this compression is restricted to the first ~250 km from the trench. Strain rates do not vary in drift mode at the active margin, which is unaffected by the distance to the upwelling. The continental lithosphere is not deformed at all excepted at the passive margin where we clearly see the influence of the upwelling. When the upwelling is closer to the passive margin ($L = 3000$ km, dashed line), the force acting on the lithosphere is bigger because the convection cell is smaller and less viscous dissipation occurs in the mantle. The deformation then decreases during ocean spreading (e.g., $L = 1000$ km, dotted line) until the system enters the collision mode. Then, strain rates dramatically increase at the active margin, further in the continent, and at the passive margin. The joint effects of upwellings and downwellings are thus essential in collision mode but not in drift mode.

4. Discussion

[33] To first order, the compression at passive margins can be reproduced under certain conditions: (i) the motion of the lithosphere above the convection cell has to be prevented or impeded by slab anchoring, continental collision, or any mechanism suited to restrain plate motion, (ii) upwellings have to be active, as the downwellings alone do not trigger compression at passive margins, (iii) the oceanic lithosphere has to be stronger than the continental lithosphere, and (iv) the viscosity ratio between the lithosphere and the upper mantle has to be ~100.

[34] Under these conditions, even our simple models yield results that agree with observations. The magnitude of compression at passive margins is likely sufficient to trigger viscous compression but also tectonic inversion, uplift and exhumation of passive margins. These models present, however, certain crude assumptions, in particular because they rely on linear viscous rheology which only varies with depth. However, the aim of this study is not to perfectly fit the data but to test the plausibility of a mechanism, i.e., to explore how upwelling and downwelling forces in the mantle stress the lithosphere, and may or may not supply the necessary conditions for passive margin inversion when the system switches from drift to collision mode.

[35] Perfectly fitting the data is outside the scope of this study, as too many unknowns such as the precise value of the total driving force, its partitioning between upwellings and downwellings, the departure from an idealized convection cell, and more accurate rheological parameters should be accounted for. In particular, the viscosity structure could be tuned because continental margins (both active and passive) are probably weaker than the continental lithosphere itself, because of the stress and temperature dependence of the rheology. By tuning such parameters, it may be possible to obtain a closer resemblance to nature, but the global dynamics will likely be the same as in our abstract models. Passive margin compression could not be achieved without a convection regime that approaches that of a sluggish lid, and without the active support from an upwelling force at the ridge side of the convection cell, in addition to the ridge-push, whose magnitude and above all, the magnitude of its temporal changes, are smaller and would not significantly alter the force balance.

[36] The simplified model setup that we designed here is mostly conceptual and does not allow for a close examination of the location of expected locations of compression. We therefore also conducted tests using more "realistic," 3-D spherical models (Figure 10), using the global mantle flow modeling setup as discussed by *Becker and Faccenna* [2011]. We explore models where mantle flow is alternatively driven by density anomalies inferred from seismic tomography—and therefore includes both downwellings at subduction zones and upwellings above the superswells—and density anomalies that correspond to subducting slabs only. While the second scenario (Figure 10a) mostly compresses the active margins of upper plates and leaves other areas at rest, the first scenario (Figure 10b) efficiently compresses passive margins where the geological record reveals their uplift, exhumation, and tectonic inversion. This confirms the conclusions from the simplified 2-D models.

[37] Such effects are particularly clear for the South American plate, where only the active margin is under compression if flow is driven by the descending Nazca slab alone, and both active and passive margins are compressed when mantle upwellings drive the system. This finding also

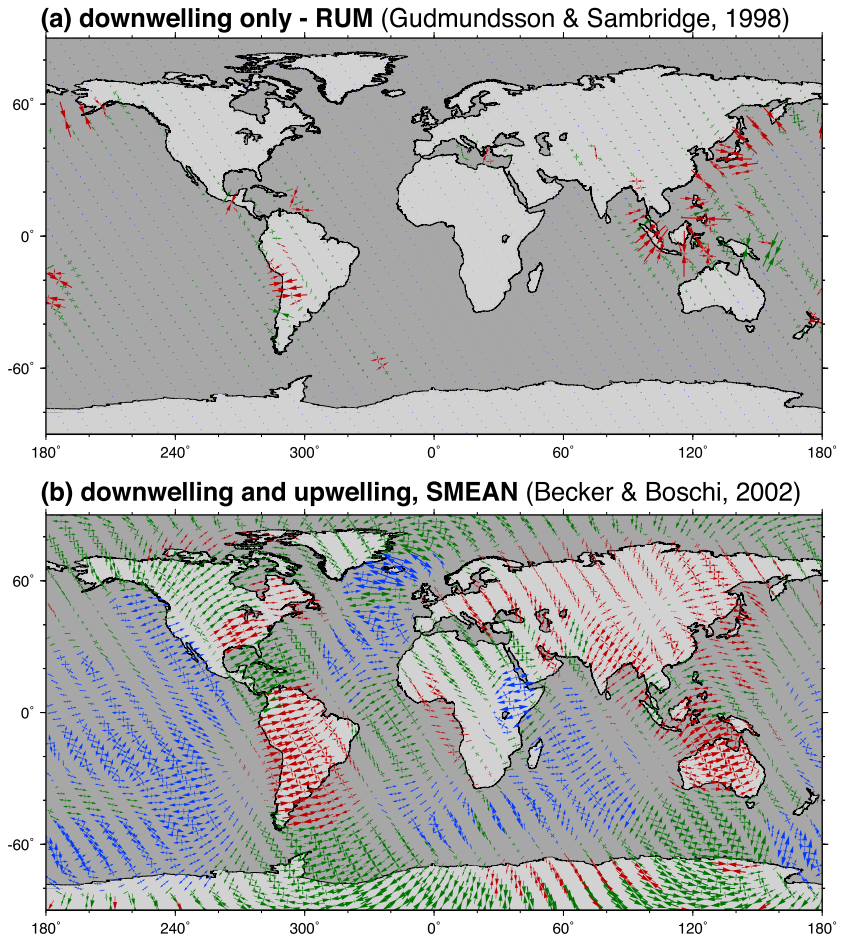

Figure 10. Global, 3-D spherical circulation models. Red, green, and blue arrows correspond to compressive, transform, and extensive areas, respectively. Arrow sizes relate to the magnitude. Results are obtained using density anomalies corresponding to (a) subducting slabs only (RUM: Regionalized upper mantle model [*Gudmundsson and Sambridge*, 1998]) and (b) results obtained when the flow include both downwellings at subduction zones and upwellings above the superswells (SMEAN: Composite *S* wave model by *Becker and Boschi* [2002]). See *Becker and Faccenna* [2011] for details.

holds along passive margins from western Africa, Eastern North America, Scandinavia and the British Isles, and in Australia, providing a good match with the examples of Figure 1. Unlike these more Earth-like global circulation models, the simplified model setup that we designed here is mostly conceptual and does not allow for a close examination of the location of expected locations of compression. The advanced regional specificity of the global models also helps to explain for instance that observed tectonic inversion and exhumation sometimes occur remotely from the strict ocean-continent boundary (Figure 1).

[38] The large-scale, deep mantle flow mechanisms that we discuss here may well interact with local, self-destabilization and subduction initiation effects at passive margins, in particular along the Atlantic [*Nikolaeva et al*., 2010, 2011]. Gravitational instabilities arise due to the effectively positively buoyant continental lithosphere, and may lead to underthrusting of the oceanic lithosphere beneath the continental lithosphere, if this latest is sufficiently weak to flow. *Nikolaeva et al*. [2010] show that such instabilities may occasionally trigger modest compression and uplift. The far-field forces due to the underlying mantle convection, that act as a vice, would facilitate this destabilization, foster underthrusting, uplift, and exhumation of the passive margin.

[39] Also, some regional settings deserve particular attention. For instance, Greenland does not clearly fit in our simplified model setup because it is surrounded by passive margins. Yet this situation is even more prone to compression (modeling shows that sea floor spreading compresses plates, subduction extends them). However, our global circulation models do not reveal compression but strike slip in the region. This result may be due to the fact that the model lacks definition for shorter wavelength patterns of mantle flow because the resolution of the input tomographic model compares to that of Greenland itself.

5. Conclusions

[40] In summary, both our simplified theoretical models and more Earth-like global circulation models reveal that the combined buoyancy forces from upwellings and downwellings play a prominent role in the tectonic reactivation of passive margins, their uplift, and exhumation. Plate convergence is assisted by pulsating deep mantle upwellings which transiently

actively stimulate plate motion at the other end, on the ridge-side. The Cenozoic is the time during which many mountain belts grew worldwide. It is also the time during which the free drift of continents above the mantle became gradually hampered by multiple collisions, like Africa-Eurasia, Arabia-Eurasia, India-Eurasia, Australia-Eurasia, and slab anchoring underneath South America [*Husson et al*., 2012]. These events are contemporaneous with the disappearance of many subduction zones (most of the Tethys and Farallon), while total ridge length remained steady. All of these events contribute to an increase of the compression in the lithosphere. Most emblematic is the development of the American cordilleras and Alpine chains. However, the same mechanism may also have led to compression at passive margins, as shown by the simultaneous morphotectonic events at passive margins (as discussed for South America by *Cogné et al*. [2012], for example). Such compressive events, both at active and passive margins, were likely boosted by active mantle upwellings. The activity of those upwellings may be somewhat irregular, leading us to suggest that morphotectonic activity at both passive and active margins is strongly affected by the transient bursts that may occur on the ridge side of tectonic plates, e.g., due to pulsating thermochemical, deep mantle plumes. Indeed, other upwelling pulses may have occurred at other times, as highlighted for instance by post-rift vertical movements and horizontal deformation observed in the eastern margin of the Central Atlantic before the Cenozoic [*Bertotti and Gouiza*, 2012]. In principle, this mechanism could thus have prevailed during other compressive phases (Hercynian, for instance), and this would be an indirect proxy to evaluate the respective roles of upwellings and downwellings in the past, as well as their geometrical distribution. Unfortunately, deformation at passive margins is most certainly too subtle to be preserved earlier than the current collision phase. For the more recent times, however, the not-so-passive margins may hold useful, and as of yet no fully exploited clues, for unraveling the dynamics of plate tectonics.

[41] **Acknowledgments.** We thank Gael Choblet for the fruitful discussions at the beginning this work. P.Y. thanks Thibault Duretz and Dave May for the help during the code development. We also highly appreciated the constructive comments of the Associate Editor, Giovanni Bertotti, an anonymous reviewer, and Peter Japsen.

References

Andersen, M. S., and L. O. Boldreel (1995), Tertiary compression structures in the Faeroe-Rockall area, *Geol. Soc. London Spec. Publ.*, *90*, 215–216.

Becker, T. W. (2006), On the effect of temperature and strain-rate dependent viscosity on global mantle flow, net rotation, and driving forces, *Geophys. J. Int.*, *167*, 943–957.

Becker, T. W., and L. Boschi (2002), A comparison of tomographic and geodynamic mantle models, *Geochem. Geophys. Geosyst.*, *3*(1), 1003, doi:10.1029/2001GC000168.

Becker, T. W., and C. Faccenna (2011), Mantle conveyor beneath the Tethyan collisional belt, *Earth Planet. Sci. Lett.*, *310*, 453–461.

Becker, T. W., and R. J. O'Connell (2001), Predicting plate velocities with mantle circulation models, *Geochem. Geophys. Geosyst.*, *2*, doi:10.1029/2001GC000171.

Bertotti, G., and M. Gouiza (2012), Post-rift vertical movements and horizontal deformations in the eastern margin of the Central Atlantic: Middle Jurassic to Early Cretaceous evolution of Morocco, *Int. J. Earth Sci.*, *101*, 2151–2165.

Bishop, P., and G. Goldrick (2000), Geomorphological evolution of the East Australian continental margin, in *Geomorphology and Global Tectonics*, edited by M. A. Summerfield, pp. 227–255, Wiley, Chichester, U. K.

Blakey, R. C. (2008), Gondwana paleogeography from assembly to breakup —A 500 m.y. odyssey, *Geol. Soc. Am. Spec. Pap.*, *441*, 1–28.

Brekke, H. (2000), The tectonic evolution of the Norwegian Sea Continental Margin with emphasis on the Vøring and Møre Basins, *Geol. Soc. London Spec. Publ.*, *167*, 327–378.

Briggs, S. E., R. J. Davies, J. Cartwright, and R. Morgan (2009), Thrusting in oceanic crust during continental drift offshore Niger Delta, equatorial Africa, *Tectonics*, *28*, TC1004, doi:10.1029/2008TC002266.

Brown, R. W., M. A. Summerfield, and A. J. W. Gleadow (2002), Denudational history along a transect across the Drakensberg Escarpment of southern Africa derived from apatite fission track thermochronology, *J. Geophys. Res.*, *107*(B12), 2350, doi:10.1029/2001JB000745.

Cizkova, H., A. P. van den Berg, W. Spakman, and C. Matyska (2012), The viscosity of Earth's lower mantle inferred from sinking speed of subducted lithosphere, *Phys. Earth Planet. Inter.*, *200–201*, 56–62.

Clift, P. D. (2010), Enhanced global continental erosion and exhumation driven by Oligo-Miocene climate change, *Geophys. Res. Lett.*, *37*, L09402, doi:10.1029/2010GL043067.

Cloetingh, S., and J. D. Van Wees (2005), Strength reversal in Europe's intraplate lithosphere: Transition from basin inversion to lithospheric folding, *Geology*, *33*, 285–288.

Cloetingh, S., F. Beekman, P. A. Ziegler, J. D. Van Wees, and D. Sokoutis (2008), Post-rift compressional reactivation potential of passive margins and extensional basins, *Geol. Soc. Spec. Publ.*, *306*, 27–70.

Cobbold, P. R., K. Meisling, and V. S. Mount (2001), Reactivation of an obliquely rifted margin, Campos and Santos basins, southeastern Brazil, *Am. Assoc. Pet. Geol. Bull.*, *85*, 1925–1944.

Cobbold, P. R., E. A. Rossello, P. Roperch, C. Arriagada, L. A. Gomez, and C. Lima (2007), Distribution, timing, and causes of Andean deformation across South America, *Geol. Soc. London Spec. Publ.*, *272*, 321–343.

Cogné, N., K. Gallagher, and P. R. Cobbold (2011), Post-rift reactivation of the onshore margin of southeast Brazil: Evidence from apatite (U-Th)/He and fission-track data, *Earth Planet. Sci. Lett.*, *309*, 118–130.

Cogné, N., K. Gallagher, P. R. Cobbold, C. Riccomini, and C. Gautheron (2012), Post-breakup tectonics in southeast Brazil from thermochronological data and combined inverse-forward thermal history modeling, *J. Geophys. Res.*, *117*, B11413, doi:10.1029/2012JB009340.

Conrad, C. P., and C. Lithgow-Bertelloni (2002), How mantle slabs drive plate tectonics, *Science*, *298*, 207–209.

Conrad, C. P., and C. Lithgow-Bertelloni (2006), Influence of continental roots and asthenosphere on plate-mantle coupling, *Geophys. Res. Lett.*, *33*, L05312, doi:10.1029/2005GL025621.

Doré, A. G., E. R. Lundin, C. Fichler, and O. Olesen (1997), Patterns of basement structure and reactivation along the NE Atlantic margin, *J. Geol. Soc.*, *154*, 85–92.

Faccenna, C., T. W. Becker, C. P. Conrad, and L. Husson (2013), Mountain building and mantle dynamics, *Tectonics*, *32*, 80–93, doi:10.1029/2012TC003176.

Fleitout, L., and C. Froidevaux (1983), Tectonic stresses in the lithosphere, *Tectonics*, *2*, 315–324.

Gallagher, K., and R. Brown (1999), The Mesozoic denudation history of the Atlantic margins of southern Africa and southeast Brazil and the relationship to offshore sedimentation, in *The Oil and Gas Habitats of the South Atlantic*, Geol. Soc. Spec. Publ., vol. 153, edited by N. R. Cameron, R. H. Bate, and V. S. Clure, pp. 41–53.

Gerya, T. V., and D. Yuen (2003), Characteristics-based marker-in-cell method with conservative finite-differences schemes for modeling geological flows with strongly variable transport properties, *Phys. Earth Planet. Inter.*, *140*, 293–318.

Gerya, T. V., and D. Yuen (2007), Robust characteristics method for modelling multiphase visco-elasto-plastic thermo-mechanical problems, *Phys. Earth Planet. Inter.*, *163*, 83–105.

Ghorbal, B., G. Bertotti, J. Foeken, and P. Andriessen (2008), Unexpected Jurassic to Neogene vertical movements in 'stable' parts of NW Africa revealed by low temperature geochronology, *Terra Nova*, *20*, 355–363.

Ghosh, A., T. W. Becker, and S. J. Zhong (2010), Effects of lateral viscosity variations on the geoid, *Geophys. Res. Lett.*, *37*, L01301, doi:10.1029/2009GL040426.

Gomes Sant'Anna, L., H. D. Schorscher, and C. Riccomini (1997), Cenozoic tectonics of the Fonseca Basin Region, eastern Quadrilátero Ferrífero, MG, Brazil, *J. South Am. Earth Sci.*, *10*, 275–284.

Gordon, R. G. (2000), Diffuse oceanic plate boundaries: Strain rates, vertically averaged rheology, and comparisons with narrow plate boundaries and stable plate interiors, in *History and Dynamics of Global Plate Motions*, Geophysical Monograph, vol. 121, edited by M. A. Richards, R. G. Gordon, and R. D. Van der Hilst, pp. 143–159, AGU, Washington, D. C.

Green, P. F., and I. R. Duddy (2010), Synchronous exhumation events around the Arctic including examples from Barents Sea and Alaska North Slope, in *Petroleum Geology: From Mature Basins to New Frontiers—Proceedings of the 7th Petroleum Geology Conference*, edited by B. A. Vining and S. C. Pickering, pp. 633–644, Geological Society, London.

Gudmundsson, O., and M. Sambridge (1998), A regionalized upper mantle (RUM) seismic model, *J. Geophys. Res.*, *103*, 7121–7136.

Gunnell, Y., and L. Fleitout (1998), Shoulder uplift of the Western Ghats passive margin, India: A denudational model, *Earth Surf. Processes Landforms*, *23*, 391–404.

Hillis, R. R., S. P. Holford, P. F. Green, A. G. Doré, R. W. Gatliff, M. S. Stoker, K. Thomson, J. P. Turner, J. R. Underhill, and G. A. Williams (2008a), Cenozoic exhumation of the southern British Isles, *Geology*, *36*, 371–374.

Hillis, R. R., M. Sandiford, S. D. Reynolds, and M. C. Quigley (2008b), Present-day stresses, seismicity and Neogene-to-Recent tectonics of Australia's 'passive' margins: intraplate deformation controlled by plate boundary forces, *Geol. Soc. Spec. Publ.*, *306*, 71–90.

Holford, S. P., P. F. Green, J. P. Turner, G. A. Williams, R. R. Hillis, D. R. Tappin, and I. R. Duddy (2008), Evidence for kilometric-scale Neogene exhumation driven by compressional deformation in the Irish Sea basin system, *Geol. Soc. Spec. Publ.*, *306*, 91–119.

Holford, S. P., J. P. Turner, P. F. Green, and R. R. Hillis (2009), Signature of cryptic sedimentary basin inversion revealed by shale compaction data in the Irish Sea, western British Isles, *Tectonics*, *28*, TC4011, doi:10.1029/2008TC002359.

Hudec, M. R., and M. P. A. Jackson (2002), Structural segmentation, inversion, and salt tectonics on a passive margin: Evolution of the Inner Kwanza Basin, Angola, *Geol. Soc. Am. Bull.*, *114*, 1222–1244.

Husson, L. (2012), Trench migration and upper plate strain over a convecting mantle, *Phys. Earth Planet. Inter.*, *212–213*, 32–43.

Husson, L., and Y. Ricard (2004), Stress balance above subduction: Application to the Andes, *Earth Planet. Sci. Lett.*, *222*, 1037–1050.

Husson, L., C. P. Conrad, and C. Faccenna (2012), Plate motions, Andean orogeny, and volcanism above the South Atlantic convection cell, *Earth Planet. Sci. Lett.*, *317–318*, 126–135.

Jackson, M. P. A., M. R. Hudec, and K. A. Hegarty (2005), The great West African Tertiary coastal uplift: Fact or fiction? A perspective from the Angolan divergent margin, *Tectonics*, *24*, TC6014, doi:10.1029/2005TC001836.

Japsen, P. (1998), Regional velocity-depth anomalies, North Sea Chalk: A record of overpressure and Neogene uplift and erosion, *AAPG Bull.*, *82*, 2031–2074.

Japsen, P., and J. A. Chalmers (2000), Neogene uplift and tectonics around the North Atlantic: Overview, *Global Planet. Change*, *24*, 165–173.

Japsen, P., J. M. Bonow, P. F. Green, J. A. Chalmers, and K. Lidmar-Bergström (2006), Elevated, passive continental margins: Long-term highs or Neogene uplifts? New evidence from West Greenland, *Earth Planet. Sci. Lett.*, *248*, 330–339.

Japsen, P., J. A. Chalmers, P. F. Green, and J. M. Bonow (2012a), Elevated, passive continental margins: Not rift shoulders, but expressions of episodic, post-rift burial and exhumation, *Global Planet. Change*, *90–91*, 73–86.

Japsen, P., J. M. Bonow, P. F. Green, P. R. Cobbold, D. Chiossi, R. Lilletveit, L. P. Magnavita, and A. J. Pedreira (2012b), Episodic burial and exhumation history of NE Brazil after opening of the South Atlantic, *GSA Bull.*, *124*, 800–816.

Jolivet, L., and C. Faccenna (2000), Mediterranean extension and the Africa-Eurasia collision, *Tectonics*, *19*, 1095–1106.

Kohlstedt, D. L., B. Evans, and S. J. Mackwell (1995), Strength of the lithosphere: Constraints imposed by laboratory experiments, *J. Geophys. Res.*, *100*, 17,587–17,602.

Kreemer, C., W. E. Holt, and A. J. Haines (2003), An integrated global model of present-day plate motions and plate boundary deformation, *Geophys. J. Int.*, *154*, 8–34.

Lavier, L. L., M. S. Steckler, and F. Brigaud (2001), Climatic and tectonic control on the Cenozoic evolution of the West African margin, *Mar. Geol.*, *178*, 63–80.

Leroy, M., O. Dauteuil, and P. R. Cobbold (2004), Incipient shortening of a passive margin: The mechanical roles of continental and oceanic lithospheres, *Geophys. J. Int.*, *159*, 400–411.

Lithgow-Bertelloni, C., and J. H. Guynn (2004), Origin of the lithospheric stress field, *J. Geophys. Res.*, *109*, B01408, doi:10.1029/2003JB002467.

Lithgow-Bertelloni, C., and P. G. Silver (1998), Dynamic topography, plate driving forces and the African superswell, *Nature*, *395*, 269–272.

Loiselet, C., J. Braun, L. Husson, C. Le Carlier de Veslud, C. Thieulot, P. Yamato, and D. Grujic (2010), Subducting slabs: Jellyfishes in the Earth's mantle, *Geochem. Geophys. Geosyst.*, *11*, Q08016, doi:10.1029/2010GC003172.

Lundin, E., and A. G. Doré (2002), Mid-Cenozoic post-breakup deformation in the 'passive' margins bordering the Norwegian-Greenland Sea, *Mar. Pet. Geol.*, *19*, 79–93.

Martill, D. M. (2007), The age of the Cretaceous Santana Formation fossil Konservat Lagerstätte of north-east Brazil: A historical review and an appraisal of the biochronostratigraphic utility of its palaeobiota, *Cretaceous Res.*, *28*, 895–920.

Masson, D. G., J. A. Cartwright, L. M. Pinheiro, R. B. Whitmarsh, M.-O. Beslier, and H. Roeser (1994), Compressional deformation at the ocean-continent transition in the NE Atlantic, *J. Geol. Soc.*, *151*, 607–613.

Mitrovica, J. X., and A. M. Forte (2004), A new inference of mantle viscosity based upon a joint inversion of convection and glacial isostatic adjustment data, *Earth Planet. Sci. Lett.*, *225*, 177–189.

Morais Neto, J. M., K. A. Hegarty, and G. D. Karner (2006), Preliminary constraints on paleotemperature and landscape evolution in and around Araripe Basin, northeastern Brazil, using apatite fission track analysis, *Bol. Geoc. Petrobras*, *14*, 113–119.

Nikolaeva, K., T. V. Gerya, and F. O. Marques (2010), Subduction initiation at passive margins: Numerical modeling, *J. Geophys. Res.*, *115*, B03406, doi:10.1029/2009JB006549.

Nikolaeva, K., T. V. Gerya, and F. O. Marques (2011), Numerical analysis of subduction initiation risk along the Atlantic American passive margins, *Geology*, *39*, 463–466.

Partridge, T. C., and R. R. Maud (1987), Geomorphic evolution of southern Africa since the Mesozoic, *S. Afr. J. Geol.*, *90*, 179–208.

Pedoja, K., et al. (2011), Relative sea-level fall since the last interglacial stage: Are coasts uplifting worldwide?, *Earth Sci. Rev.*, *108*, 1–15.

Peron-Pinvidic, G., G. Manatschal, S. M. Dean, and T. A. Minshull (2008), Compressional structures on the West Iberia rifted margin: Controls on their distribution, *Geol. Soc. Spec. Publ.*, *306*, 169–183.

Piasecki, S., L. M. Larsen, A. K. Pedersen, and G. K. Pedersen (1992), Palynostratigraphy of the Lower Tertiary volcanics and marine clastic sediments in the southern part of the West Greenland Basin: Implications for the timing and duration of the volcanism, *Grønlands Geol. Und. Rapp.*, *154*, 13–31.

Riccomini, C., and M. Assumpcao (1999), Quaternary tectonics in Brazil, *Episodes*, *22*, 221–225.

Ritchie, J. R., H. Johnson, M. F. Quinn, and R. W. Gatliff (2008), The effect of Cenozoic compression within the Faroe-Shetland Basin and adjacent area, *Geol. Soc. Spec. Publ.*, *306*, 121–136.

Roberts, G. G., and N. White (2010), Estimating uplift rate histories from river profiles using African examples, *J. Geophys. Res.*, *115*, B02406, doi:10.1029/2009JB006692.

Rodriguez, J. F. R., and R. Littke (2001), Petroleum generation and accumulation in the Golfo San Jorge Basin, Argentina: A basin modeling study, *Mar. Pet. Geol.*, *18*, 995–1028.

Smallwood, J. R. (2008), Uplift, compression and the Cenozoic Faroe-Shetland sediment budget, *Geol. Soc. Spec. Publ.*, *306*, 137–152.

Steinberger, B., H. Schmeling, and G. Marquart (2001), Large-scale lithospheric stress field and topography induced by global mantle circulation, *Earth Planet. Sci. Lett.*, *186*, 75–91.

Thomson, K., P. F. Green, A. G. Whitham, S. P. Price, and J. R. Underhill (1999), New constraints on the thermal history of North-East Greenland from apatite fission-track analysis, *GSA Bull.*, *111*, 1054–1068.

Turcotte, D. L., and G. Schubert (1982), *Geodynamics: Applications of Continuum Physics to Geological Problems*, 450 pp., J. Wiley, New York.

Wdowinski, S., and R. J. O'Connell (1991), Deformation of the Central Andes (15°−27°S) derived from a flow model of subduction zones, *J. Geophys. Res.*, *96*, 12,245–12,255.

Yamato, P., R. Tartèse, T. Duretz, and D. A. May (2012), Numerical modelling of magma transport in dykes, *Tectonophysics*, *526–529*, 97–109.

Yoshida, M., and T. Nakakuki (2009), Effects on the long-wavelength geoid anomaly of lateral viscosity variations caused by stiff subducting slabs, weak plate margins and lower mantle rheology, *Phys. Earth Planet. Inter.*, *172*, 278–288.